J Mater Sci (2022) 57:6607–6618

Ceramics

Noble metals Pt, Au, and Ag as nucleating agents in BaO/SrO/ZnO/SiO_2 glasses: formation of alloys and core–shell structures

Christian Thieme[1,*], Liliya Vladislavova[2], Katrin Thieme[1], Christian Patzig[1], Thomas Höche[1], and Christian Rüssel[2]

[1] Fraunhofer-Institut für Mikrostruktur von Werkstoffen und Systemen IMWS, Walter-Hülse-Straße 1, 06120 Halle (Saale), Germany
[2] Otto-Schott-Institut für Materialforschung, Jena University, Fraunhoferstraße 6, 07743 Jena, Germany

Received: 14 January 2022
Accepted: 21 February 2022
Published online: 21 March 2022

ABSTRACT

Noble metals such as Ag can be used as nucleation agents in glass ceramics. In glasses, it is incorporated predominantly as Ag^I. At temperatures slightly above the glass transition temperature, T_g, Ag^I reacts with Sb^{III} to Sb^V and metallic Ag. Usually, face-centered cubic Ag particles are nearly spherical and get facetted during crystal growth. By contrast, in the case of BaO/SrO/ZnO/SiO_2 glasses, silver has, in comparison to other noble metals, another significant, yet different effect. It forms metallic particles (hexagonal phase) with plate-like morphology during thermal treatment at 675 °C. In the second step of thermal treatment at 760 °C, this phase most probably expels some metallic Sb, which is oxidized by Sb^V (present in the surrounding glass phase) to Sb^{III}. As a result, the plate-like morphology is maintained and a crystalline shell around the metallic core is formed, mainly consisting of ZnO with some SiO_2 and antimony oxide, as proved by scanning transmission electron microscopy combined with energy-dispersive X-ray spectroscopy. This shell triggers the volume crystallization of $Ba_{0.5}Sr_{0.5}Zn_2Si_2O_7$, a phase with low thermal expansion. By comparison, alloying of Au with Sb does not occur according to the phase diagram. Instead, a thermal treatment at temperatures slightly above T_g leads to nanocrystalline, spherical Au particles. Hence, alloying and subsequent decomposition of the alloy is a prerequisite for the formation of plate-like noble metal particles.

Handling Editor: M. Grant Norton.

Address correspondence to E-mail: christian.thieme@imws.fraunhofer.de

https://doi.org/10.1007/s10853-022-07054-6

Introduction

In many glass compositions, noble metals act as nucleating agents, and the nucleation efficiency is strongly affected by the number and size of the noble metal particles [1–3]. Therefore, the presence of antimony is quite essential for the effect of noble metals as nucleation agents in many glass compositions. This has recently been shown for glasses in the system $BaO/SrO/ZnO/SiO_2$ (denoted in the literature as LEAZit, which is an acronym for **L**ow **E**xpansion **A**lkaline Earth **Zi**nc Silica**t**es) [4, 5].

Antimony in glasses is a polyvalent element and may occur in the oxidation states + III and + V. Under extremely reducing conditions, it might additionally appear as metallic antimony. In the presence of noble metals, alloying with metallic antimony can take place, and hence, the reduction of Sb^V occurs at less reducing conditions, due to the Gibbs free mixing energy of the noble metal and antimony. In any glass melt composition, the Sb^V/Sb^{III}-ratio is shifted to lower values with increasing temperature [6–8]. This is utilized in glass technology, where antimony is, first of all, a fining agent. During the fining reaction, Sb^V is reduced to Sb^{III} and gaseous oxygen is formed.

Antimony is added to glass melts in order to remove bubbles from the melt because the released oxygen diffuses into small bubbles which are still present from the melting process. This leads to a growth of the bubbles, which then ascend much faster to the surface of the melt, as their velocity increases with the square of their diameter. This reaction starts at a temperature which is affected by the glass composition. As an example, in (widely produced) soda-lime-silicate melts, this process starts at around 1,150 °C. The maximum of this reaction, i.e., the maximum of the oxygen release, is shifted to higher temperatures with increasing alkaline and alkaline earth concentrations [9]. Thermodynamic data, however, are only available in the literature for a few glass compositions, such as soda-lime-silicate and borosilicate compositions [6–8]. Nevertheless, in most silicate glasses, at the maximum temperatures supplied during melting, antimony should predominantly occur as Sb^{III}.

Noble metals, such as silver, gold, or platinum occur in glasses and melt as metals or in an oxidized state, i.e. as Ag^+, Au^+, or Pt^{2+} [10–15]. The redox equilibria generally depend on temperature; however, this effect is very different for different polyvalent elements. Hence, also redox equilibria between different polyvalent elements may shift with temperature. The studies presented in this paper were performed in compositions based on the $BaO/SrO/ZnO/SiO_2$ system, from which the crystalline phase $Ba_{0.5}Sr_{0.5}Zn_2Si_2O_7$ can be precipitated. As recently reported, this phase shows a low coefficient of thermal expansion and hence is suitable to prepare glass–ceramics or ceramics with zero thermal expansion and high thermal shock resistance [16–18].

In the following, utilizing cutting-edge microstructure diagnostics, it will be shown that the addition of antimony does not only affect the redox state of the noble metals but may also change the morphology of the noble metal particles. Moreover, the reduction of antimony to the metallic state will be also considered and discussed, taking into account the possible formation of alloys of antimony and noble metals.

The main goal of this paper is to verify a new mechanism of glass crystallization, which involves different temperature-dependent redox reactions and furthermore a third phase in between the nuclei and the main crystalline phase. It is a further goal to explain why different noble metals show very different effects.

Experimental procedure

Glasses based on the composition 8 BaO·8 SrO·34 ZnO·48.2 SiO_2·1.5 Sb_2O_3·0.3 Ag [mol%] were melted from reagent grade raw materials $BaCO_3$, $SrCO_3$, ZnO, Sb_2O_3, $AgNO_3$, and SiO_2. Around 400 to 500 g of the respective glass compositions were melted at 1,300 to 1,400 °C in an induction furnace using a Pt-crucible. Afterward, the glass melt was stirred for 1.5 to 2.0 h using a rotation frequency of up to 100 min^{-1} and then cast into a mold. Subsequently, the mold was transferred into a cooling furnace preheated to a temperature slightly above the glass transition temperature of the respective glass and then the furnace was switched off. The glass cooled slowly to room temperature with approximately 2–3 K/min. Glasses with additions of Pt were melted in a similar way. For this purpose, 0.005 and 0.01 mol% Pt were added to the following glass composition: 8 BaO·8 SrO·34 ZnO·49.5 SiO_2·0.5 Sb_2O_3. In order to obtain a

homogeneous Pt distribution within the glass batch, $PtCl_4$ was used as raw material, which was dissolved in acetone and afterward added to the batch, followed by thorough mixing and subsequent drying.

Microstructural analyses were performed using scanning transmission electron microscopy (STEM). Those analyses were performed using a FEI TITAN^3 80–300 STEM instrument operated at 300 kV and equipped with a high-angle annular dark-field detector (HAADF, Fischione Model 3000) and an energy-dispersive X-ray spectrometry (EDXS) detector (four SDD detectors, FEI company).

Mechanical wedge-polishing, after gluing thin sample pieces to a Mo half-ring as support structure, was applied to obtain electron-transparent samples using the grinding and polishing tool Multiprep™ (Allied High Tech Products, Inc.). An Ar^+ ion broad-beam milling step (precision ion polishing system PIPS, Gatan company) was performed in order to remove polishing residues and to achieve electron transparent sections of the wedge-shaped sample free of artifacts from mechanical grinding and polishing. In order to prevent static charging under electron irradiation, the sample was selectively coated with a carbon film only fractions of a nanometer-thick using 3D-Micromac's coatMASTER [19].

Results

The microstructure of a glass with the mol% composition 8 BaO·8 SrO·34 ZnO·48.2 SiO_2·1.5 Sb_2O_3·0.3 Ag thermally treated at 675 °C for 30 h is shown in Fig. 1. The morphology of the Ag nanocrystals is no more that of a crystal with a cubic space group, but that of a platelet.

Elemental distributions based on STEM EDXS (see Fig. 2) show a plate-like crystal that is highly enriched in Ag. All the other elements except for Sb are depleted within this crystal.

During a second heat treatment step, carried out at 760 °C (i.e., at a temperature higher than in the first step) for 5 h, the microstructure undergoes significant changes (see Fig. 3). Around plate-like, metallic Ag particles, oxidic shells containing Zn, Sb, and Si are observed by EDXS. Those shells are depleted in Ba and Sr. Careful quantification of subsets of EDXS mappings show that on average the shell has, under the assumption that the oxidation state of antimony is Sb^V, the following composition: $Si_{0.583}Zn_2Sb_{0.33}O_4$,

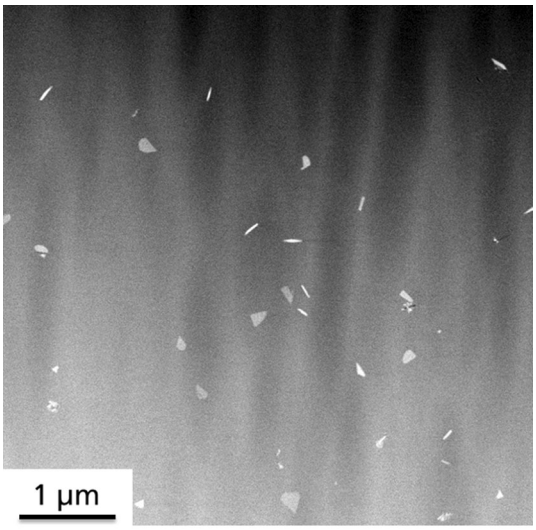

Figure 1 Large-scale micrograph of a glass bulk with the composition 8 BaO·8 SrO·34 ZnO·48.2 SiO_2·1.5 Sb_2O_3·0.3 Ag (in mol%), after heat treatment at 675 °C for 30 h obtained via STEM in HAADF mode.

while the core consists of metallic Ag. Unfortunately, the former phase cannot be found in crystal structure databases such as ICSD. Therefore, indexing of the diffraction patterns is not viable due to the lacking of reference structures to compare experimental diffraction patterns with.

The core consists of metallic silver, which can be seen in the spectra depicted in Fig. 4, the latter were collected in the marked areas shown in the left panel of Fig. 4. Furthermore, a high-resolution micrograph is shown in Fig. 5, where lattice planes are visible. The distance between those planes was measured to be 2.4 Å, which is, within the limits of calibration errors, identical to the distance of the {111} planes in crystalline Ag, which is 2.36 Å. The shell is also crystalline, which was proven via selected-area electron diffraction, SAED.

Observations made in the Ag/Sb nucleated system are in notable contrast to those previously reported from the same glass system in which Pt/Sb and Au/Sb were used for nucleation [20, 21]. The usage of those other noble metals always resulted in the formation of approximately spherical particles. In Fig. 3, also a $Ba_{1-x}Sr_xZn_2Si_2O_7$ crystal can be seen, which surrounds the Ag-containing structure. However, during TEM-analysis, those LEAZit crystals show microstructural changes due to the effect of the electron beam. The core and the shell, on the contrary, do not change during TEM analysis.

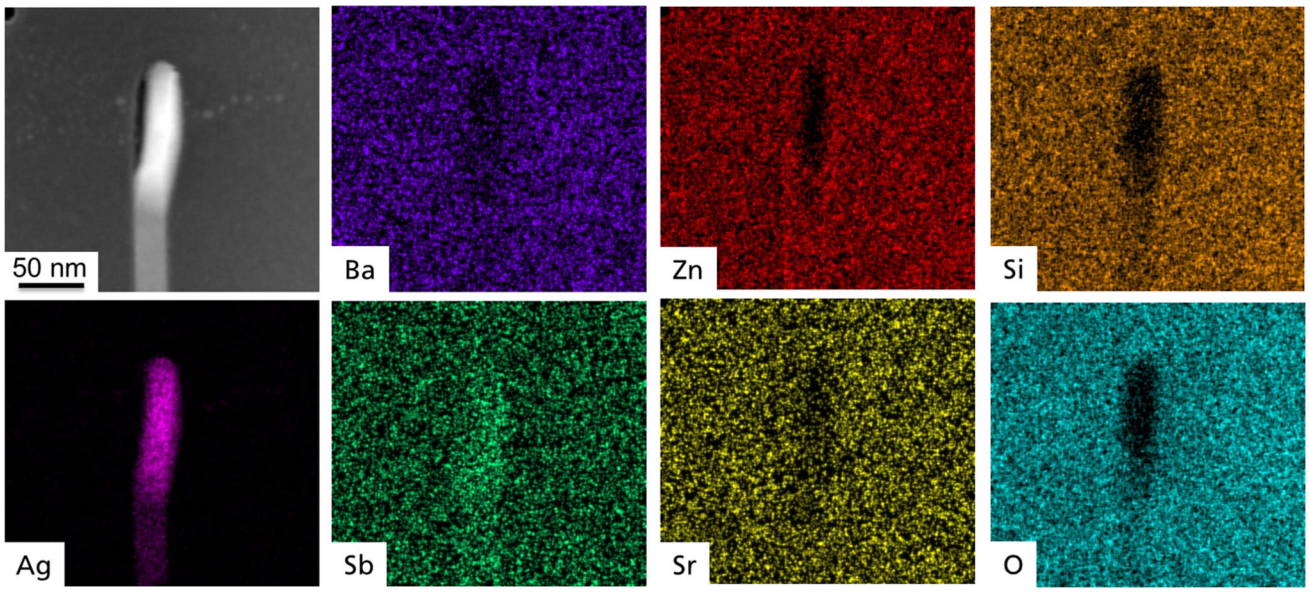

Figure 2 STEM analysis of a sample with the composition 8 BaO·8 SrO·34 ZnO·48.2 SiO_2·1.5 Sb_2O_3 0.3 Ag (in mol%), thermally treated at 675 °C for 30 h. Elemental distribution maps measured via STEM EDXS are given for Ba, Zn, Si, Ag, Sb, Sr, and O. Moreover, the corresponding HAADF micrograph is shown (top left). For each micrograph, intensity clipping was made so that visibility gets improved but quantitative information (e.g. on relative element content) cannot be derived. Less intense signals typically lead to noisier appearance.

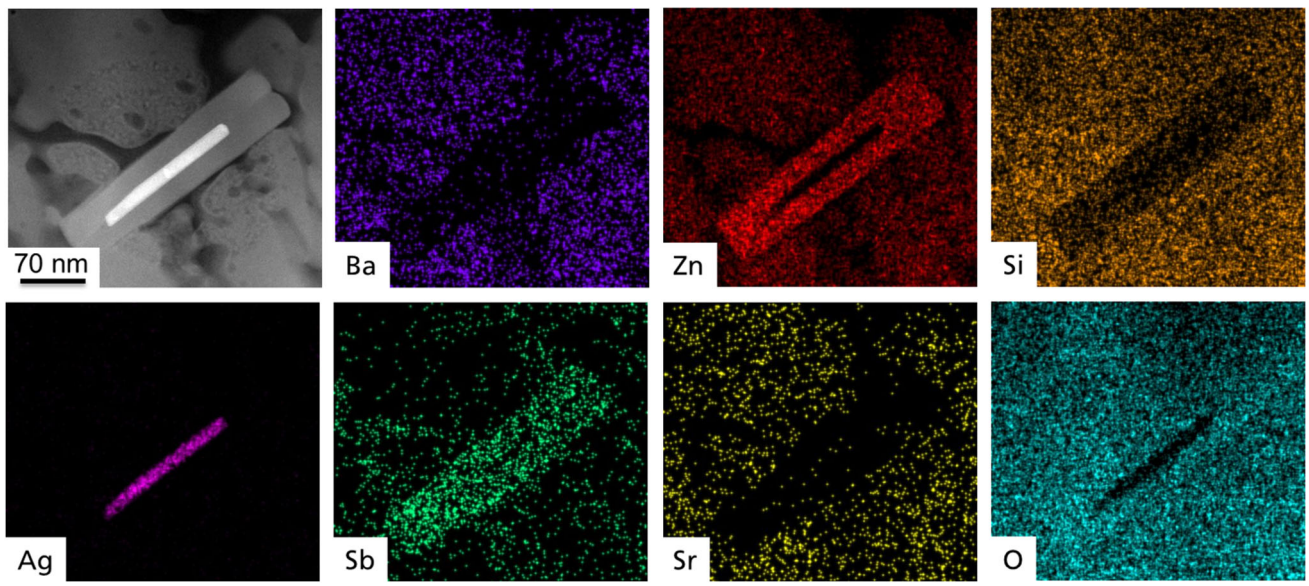

Figure 3 STEM micrograph of a sample with the composition 8 BaO·8 SrO·34 ZnO·48.2 SiO_2·1.5 Sb_2O_3· 0.3 Ag (in mol%) nucleated at 675 °C for 10 h and grown at 760 °C for 5 h. The HAADF micrograph (top left), as well as the elemental distribution maps of Ba, Zn, Si, Ag, Sb, Sr, and O, are shown.

Discussion

Formation of metallic particles in glass

The formation of nanosized metallic particles in glasses has frequently been described in the literature [1–3, 22, 23]. In these studies, the morphology of the particles does not deviate much from a cubic or spherical shape (see e.g. Ref. [4]), but the crystals may also show facets as the particles grow to larger sizes. The formation of plate-like morphologies is very

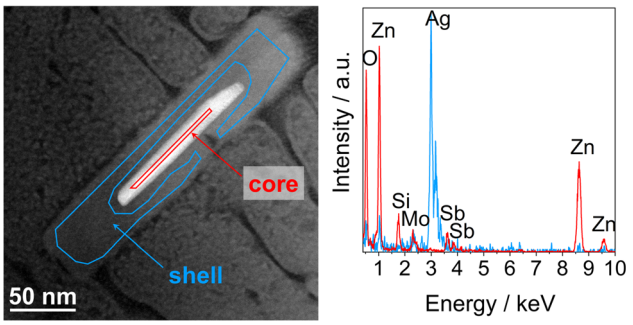

Figure 4 STEM micrograph together with the EDXS spectra of core and shell. The areas from which the spectra were taken are marked in blue and red color, in correspondence with the color representation of the spectra. The intensities of the spectra are normalized to the Mo-signal, which results as stray signal from the Mo half-ring onto which the actual TEM sample was glued.

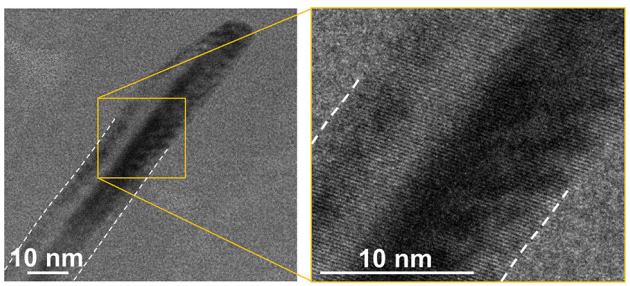

Figure 5 TEM micrograph of a silver core proving crystallinity. The dashed white lines mark a part of the border between core and shell.

uncommon for a metal with a cubic crystal lattice. In the following, it will be discussed why such morphologies cannot be observed in glasses doped with gold or platinum, although also from such glasses small metallic particles are precipitated under similar conditions.

To the best of our knowledge, the formation of core–shell structures in glasses with metallic cores and oxidic shells as thick as shown in Figs. 3 and 4 has up to now only been reported for the BaO/SrO/ZnO/SiO_2 system [5, 24].

At typical glass melting temperatures (i.e. at 1,300 to 1,650 °C), Ag, Au, or Pt occur as Ag^+ [15], Au^+ [20] or Pt^{2+} [22], or already as metallic particles. In the presence of antimony, the fining reaction leads to a high oxygen partial pressure and hence thorough oxidation of eventually present metallic particles, at least in the cases of the noble metals Ag and Au.

Upon cooling, the situation changes and in the presence of antimony, redox reactions may take place. The thermodynamics of the following redox reactions:

$$2Sb^{5+} + 2O^{2-} \rightarrow 2Sb^{3+} + O_2 \quad (1)$$

$$4Sb^{3+} + 6O^{2-} \rightarrow 4Sb^{0} + 3O_2 \quad (2)$$

can directly be measured in glass melts at high temperatures by voltammetric methods [6–8, 15] using platinum electrodes. Especially square wave voltammetry is described in the literature to enable the determination of standard potentials directly at glass melting temperatures, i.e., in the range from 850 to 1,600 °C. Using this method, standard potentials can also be measured as a function of temperature. As e.g. reported in Ref. [6], current–potential curves recorded using square wave voltammetry at high temperatures in Sb-doped melts exhibit two maxima which are attributed to the redox reactions according to Eqs. 1 and 2. The potentials attributed to these maxima are identical with the standard potentials of the respective redox pairs. In Fig. 6, the standard potentials of the Sb^{III}/Sb^{V} and the Sb^{0}/Sb^{III} redox pairs are shown as a function of temperature for a soda-lime-silica glass melt. It should be noted that the thermodynamics of the Sb^{0}/Sb^{III} redox pair is strongly affected by the electrode material, i.e., whether there is the formation of an alloy or not, or more strictly spoken by the Gibbs free mixing energy of metallic antimony in the respective electrode material. For example, standard potentials measured

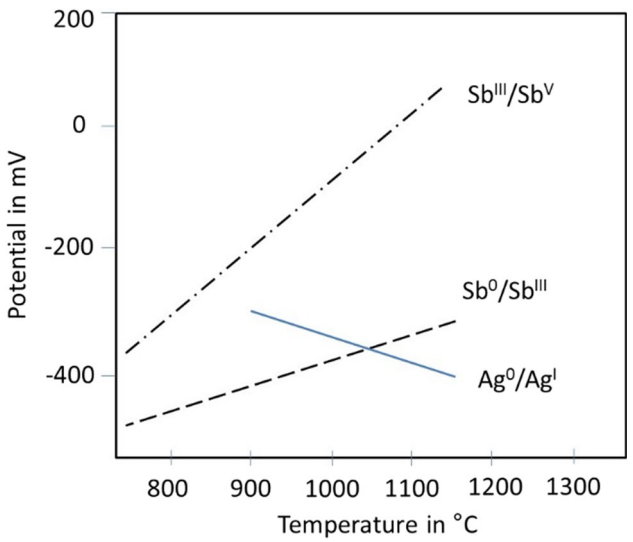

Figure 6 Standard potentials of the Sb^{III}/Sb^{V}, the Sb^{0}/Sb^{III} as well as of the Ag^{0}/Ag^{I} redox pair shown as a function of temperature (redrawn from [6, 15]), measured with platinum electrodes.

at an iridium electrode, where according to the phase diagram [25] alloy formation does not take place, were much more negative [26] than in the case of platinum electrodes.

Figure 6 also shows the thermodynamics of the redox pair Ag^0/Ag^I. Below around 1,150 °C, the standard potential decreases with increasing temperature, which is in contrast to the standard potentials of the Sb-redox pairs and to all other redox pairs up to now measured in glass melts. This means, the oxidized state, i.e. Ag^I, is favored at higher temperature. Generally, the interaction between the redox pairs will change with temperature. It should be noted that the Sb^0/Sb^{III} potentials are affected by the electrode material (alloy formation of Pt and Sb, see later) while the Sb^{III}/Sb^V (all species are dissolved in the melt) as well as of the Ag^0/Ag^I potentials (Ag and Pt do not form alloys) are not.

In principle, redox reactions will always take place, if two (or more) types of polyvalent elements are present [27–35] and the temperature changes. This has experimentally been shown for redox components, such as $Fe^{2+}/Fe^{3+}/As^{III}/As^V$ [27], $Cu^+/Cu^{2+}/Sb^{III}/Sb^V$ [28], $Cu^+/Cu^{2+}/As^{III}/As^V$ [29, 30], $Cu^+/Cu^{2+}/Fe^{2+}/Fe^{3+}$ [31], $Fe^{2+}/Fe^{3+}/Mn^{2+}/Mn^{3+}$ [31, 32], and $Mn^{2+}/Mn^{3+}/Cr^{3+}/Cr^{+6}$ [33, 34]. These studies were performed either by high-temperature UV–vis-NIR [27–31, 33, 34] or by high-temperature EPR spectroscopy [32]. It has further been reported that these equilibria are successively shifted during cooling until they are finally frozen at temperatures around T_g. In the temperature range T_g-100 K < T < T_g + 100 K, the redox state is affected by kinetics [35] and hence also by the cooling rate. Numerical simulations of redox reactions during cooling have been performed on the basis of experimentally measured thermodynamic data [35]. There, a diffusion-controlled reaction was assumed and experimentally determined diffusion coefficients [36, 37] of the respective redox species were used. These simulations showed a good agreement with the measured shift of the redox reactions and also quantitatively explained the observed freezing.

In the cases regarded in this study, besides antimony also silver, gold, or platinum are present in the respective glass compositions. Hence, besides the redox reactions of antimony described by Eqs. 1 and 2, the following reactions contribute:

$$4Ag^+ + 2O^{2-} \rightarrow 4Ag + O_2 \quad (3)$$

$$4Au^+ + 2O^{2-} \rightarrow 4Au + O_2 \quad (4)$$

$$2Pt^{2+} + 2O^{2-} \rightarrow 2Pt + O_2 \quad (5)$$

As a sum, the following reactions may take place upon cooling:

$$2Ag^+ + Sb^{3+} \rightleftarrows 2Ag + Sb^{5+} (3) - (1) = (6) \quad (6)$$

$$2Au^+ + Sb^{3+} \rightleftarrows 2Au + Sb^{5+} (4) - (1) = (7) \quad (7)$$

$$Pt^{2+} + Sb^{3+} \rightleftarrows Pt + Sb^{5+} (5) - (1) = (8) \quad (8)$$

On cooling, these reactions are shifted to the right-hand side. This can be shown for Eq. 6 by the thermodynamic data reported in the literature [6, 15].

For Eqs. 1 and 3, equilibrium constants, $K_1(T)$ and $K_3(T)$ can respectively be defined. The equilibrium constant of Eq. 6, $K_6(T)$, is then given by: $K_6(T) = K_3(T)/K_1(T)$. From $RT \ln(K(T)) = -\Delta G^0 = -\Delta H^0 + T\Delta S^0$ follows (with: ΔG^0 = standard Gibbs free energy, ΔH^0 = standard reaction enthalpy, and ΔS^0 = standard reaction entropy):

$$K_6(T) = \frac{K_3(T)}{K_1(T)} = exp\left[\left(-\Delta G_3^0(T) + \Delta G_1^0(T)\right)/(RT)\right] = exp\left[\left(-\Delta H_3^0 + \Delta H_1^0\right)/(RT)\right] \cdot exp\left[\left(\Delta S_3^0 - \Delta S_1^0\right)/R\right] \quad (9)$$

$$\mathrm{Term}(A) = exp\left[\left(-\Delta H_3^0 + \Delta H_1^0\right)/(RT)\right]$$

$$\mathrm{Term}(B) = exp\left[\left(\Delta S_3^0 - \Delta S_1^0\right)/R\right]$$

The term (B) does (to a first approximation) not depend on temperature; the $\Delta H°_1$-value of Eq. 1 has been reported to be 169 kJ·mol^{-1} for a soda-lime-silicate melt [6] while $\Delta H°_3$ is negative [15]. Hence, $(-\Delta H°_3 + \Delta H°_1)$ is positive and $K_6(T)$ increases with decreasing temperature. Then the equilibrium according to Eq. 6 is shifted to the right upon cooling, i.e., metallic silver is preferred during cooling if Sb^{III} is present. If Sb^{III} is not present, silver remains in the oxidation state Ag^+ due to a lack of a reaction partner. In this context, it should be mentioned, that the physical solubility of elemental oxygen in glass is much too low to noticeably affect the redox equilibrium [38] in the case of glasses containing 0.3 mol% silver.

It can also be seen by the deeper coloration of a glass (yellow to brown), which is attributed to a higher quantity of metallic silver, if to the same initial Ag_2O concentration in the batch, an excess of antimony oxide is added [5]. Thermal treatments at temperatures slightly above T_g result in a deeper

coloration in Ag (yellow) as well as in Au (red) containing glasses due to the plasmonic resonance of Au- and Ag-clusters with diameters in the nanometer range. The same base applies for Pt, where the grey coloration was strongly dependent on the added Pt concentration as well as on the size of the Pt clusters. Adding Sb_2O_3 leads to the reduction of Pt^{2+} in the glass during thermal treatment [4].

For Eqs. 4 and 5, thermodynamic data are unfortunately not reported in the literature. Nevertheless, the intensity of the red coloration of the BaO/SrO/ZnO/SiO_2 glasses which solely contain gold and no antimony is much less (or negligible) than in glasses, containing both gold and antimony [20]. This is a strong indication that also the reaction according to Eq. 7 is shifted to the right when cooling.

During re-heating of ruby glasses with nano-sized noble metal crystals at temperatures well above the glass transition temperature but well below the synthesis temperature of the glass, the mean size of the particles gets smaller again, which is a proof of the shift in the redox reaction [20]. Here, it can clearly be concluded that with increasing temperature, the redox reaction is shifted towards Au^+ and Sb^{III}.

Morphology and alloy formation

Nevertheless, the redox reactions according to Eqs. 6, 7, 8 do not explain the differences in the behavior of the different noble metals during their precipitation from glasses. In the following, the phase diagrams of noble metal/antimony are described in order to see whether alloying of the noble metal and elemental antimony may also affect formation of metallic particles as well as crystallization.

The system Pt/Sb

The phase diagram Pt/Sb has a deep eutectic point at the composition $Pt_{0.71}Sb_{0.29}$ attributed to a temperature of 633 °C [39]. Hence, this eutectic should have a strongly negative Gibbs free mixing energy. Minor quantities of antimony are also soluble in metallic platinum. For example, at a temperature of 755 °C ca. 7 at%, Sb can be dissolved in the cubic platinum lattice. This temperature is within the range used for nucleation and crystallization for many glass compositions. This is in agreement with EDXS analyses of precipitated platinum particles which show only minor Sb concentrations [4], so binary compounds such as Pt_4Sb should not play any role during precipitation of platinum nanoparticles from glass, at least under conditions usually applied.

Upon cooling, the following reactions may take place:

$$5Sb^{3+} \rightarrow 3Sb^{5+} + 2Sb \tag{10}$$

$$xSb^{3+} + xPt^{2+} \rightarrow xSb^{5+} + xPt \tag{11}$$

$$2Sb + xPt \rightarrow Sb_2Pt_x \tag{12}$$

$$(5+x)Sb^{3+} + xPt^{2+} \rightarrow (3+x)Sb^{5+} + Sb_2Pt_x \quad (10) + (11) + (12) = (13) \tag{13}$$

The compound Sb_2Pt_x (with $x > 29$) stands for a solid solution, which has a cubic crystal structure (space group $Fm\bar{3}m$) and contains mainly Pt and some Sb ($\leq$ 7 wt%).

Since antimony should predominantly occur as Sb^{III} at high temperatures, it might undergo disproportionation to Sb^{V} and elemental Sb (Eq. 10). Otherwise, during cooling, it reduces Pt^{2+} (which is supposedly the most stable oxidized platinum species) to the metal (Eq. 11). Finally, Pt and Sb form an alloy (Eq. 12), which is thermodynamically favored due to the highly negative Gibbs free mixing energy (–135 kJ/mol [26]). These reactions should not be consecutive, but concurrent steps. In summary (see Eq. 13), this easily explains why some enrichment of Sb in the platinum particles may occur. These solid solutions have the cubic space group $Fm\bar{3}m$, i.e., the same as pure platinum.

Figure 7 shows the number of platinum particles as a function of time determined in a glass with the mol% composition 8 BaO·8 SrO·34 ZnO·49.5 SiO_2·0.5 Sb_2O_3 and additionally 0.005 or 0.01 mol% Pt. The number of particles was determined using laser scanning microscopy (LSM) and the procedure is described in detail in Ref. [4]. It is seen that the number of crystals and hence probably also the number of platinum particles increases steadily during thermal treatment at 700 °C (T_g = 680 °C) for times of up to 24 h (see Fig. 7). Scanning electron microscopy (SEM) and EDXS showed that Pt/Sb alloys are formed. That means that the platinum particles in the presence of antimony are (at least) not solely formed during cooling but during thermal treatment at a temperature 20 K above T_g. In Fig. 7, also the platinum concentration is varied (0.005 and 0.01 mol% Pt). It should be noted that the number of particles for the twice as high Pt concentration is

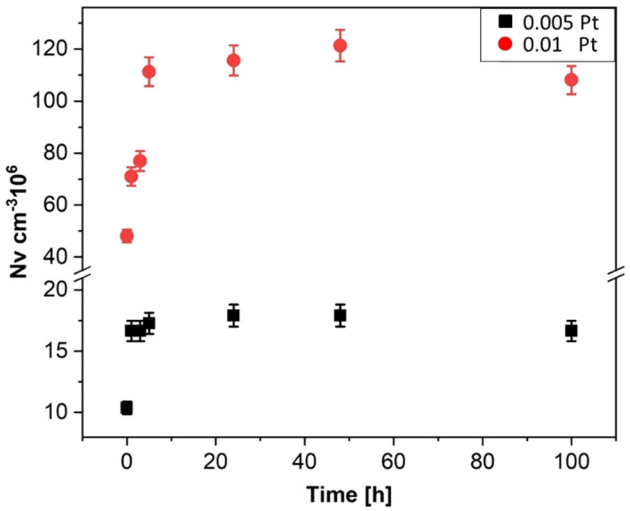

Figure 7 Number of crystals per unit volume as a function of the nucleation time for samples containing 0.005 and 0.01 mol% Pt after thermal treatment at 700 °C [4].

approximately about seven times higher. As the size of the platinum particles does not differ much, this is evidence that a certain concentration of platinum is soluble in the melt under the conditions prevailing. The reaction according to Eq. 13 does not lead only to an alloying of Sb with Pt, but should also lead to a higher Sb^{V}/Sb^{III} ratio near the Pt particles, due to limited diffusion.

The system Au/Sb

The phase diagram Au/Sb [40] is notably different from the Pt/Sb diagram. Although there is also a eutectic, the solubility of Sb in Au at 700 °C is around 1 wt% and hence notably smaller than that in Pt. The second difference is that Au-rich, binary compounds do not occur. The compound $AuSb_2$ is the only binary compound in this phase diagram. In a recent publication, it was shown that in the gold and antimony doped $BaO/SrO/ZnO/SiO_2$ glasses, any hint at alloying of the gold nanoparticles with antimony was not obtained [20]. In analogy, the calculations of the wavelengths attributed to the plasmonic resonance were in agreement with the dielectric function of gold, using the mean particle sizes determined by TEM. Alloying of the gold to a notable extent should change the dielectric function and hence, also the plasmonic resonance. The voltammetric peak potentials of the Sb^{III}/Sb^{V} redox equilibrium measured at a gold electrode are approximately the same as those measured at an Ir-electrode, which, according to the phase diagram, does not show alloying with Sb [26]. This is another hint that an Au/Sb alloy is not formed.

According to experimental studies, antimony notably facilitates the precipitation of gold nanoparticles and hence the formation of the ruby color [20]. If adding antimony to the glass batch, a much more intense coloration is obtained under the same thermal conditions. Hence, the initially formed Au^{+} is reduced by Sb^{III}, and metallic gold as well as Sb^{V} are formed according to Eq. 7.

As a consequence, the effect of antimony on the precipitation of gold nanoparticles should be that the redox equilibrium is shifted to the Au^{0}-rich side (see Eq. 7) during cooling. If the glass is heated to temperatures just above T_g, gold atoms cluster and form nanoparticles which give rise to the red coloration. If too high temperatures are reached, the Au^{0} species are oxidized by Sb^{V} and completely dissolve again in the glass melt as Au^{+} while Sb^{3+} is formed.

The system Ag/Sb

To the best of our knowledge, all commercial glasses from which nanocrystalline silver can be precipitated, such as photothermal refractive glasses, usually contain alumina [41, 42]. The lack of alumina in the glasses considered in this paper changes thermodynamics notably. By contrast to all studies on other polyvalent elements in glass melts, the Ag^{+}/Ag^{0} equilibrium in glasses without alumina is shifted to the oxidized state with increasing temperatures [15].

The phase diagram Ag/Sb is reported in Ref. [43] and a part of it is depicted in Fig. 8. In analogy to the other phase diagrams discussed here, a deep eutectic occurs. The phase diagram shows two binary compounds. In contrast to the cubic lattice of metallic Ag (space group: $Fm\bar{3}m$), the two binary compounds with the nominal compositions $Ag_{0.84}Sb_{0.16}$ and $Ag_{0.79}Sb_{0.21}$ are hexagonal and orthorhombic with the space groups $P6_3/mmc$ and Pmm2, respectively [44]. Furthermore, at 700 °C, up to 7 at% antimony can be dissolved in the silver lattice without changing the space group ($Fm\bar{3}m$). With further increasing antimony concentrations, the hexagonal phase should first additionally be formed and with increasing antimony concentration exclusively be found.

Unfortunately, results from voltammetric measurements of antimony doped glasses with silver electrodes are not reported and can scarcely be

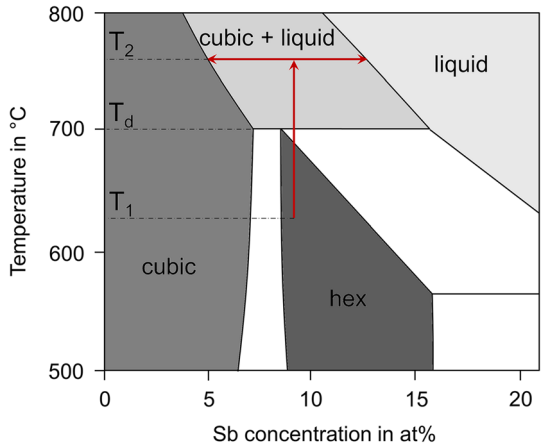

Figure 8 Part of the Ag/Sb phase diagram [43]. At T_1, the hexagonal phase is formed and after re-heating to T_2, this phase decomposes into the cubic Ag-rich phase and the liquid (red arrow).

obtained considering the low melting point of silver (961 °C) which restricts the maximum temperature for voltammetric measurements to around 800 °C, which for most glass compositions is strictly impossible due to the much too high viscosities at such temperatures.

In the following, it is first assumed, that according to the mechanism already described for the case of Pt/Sb, during the first step of thermal treatment, at 675 °C (temperature T_1 in Fig. 8), an Sb containing alloy with an Sb concentration above the solubility limit of Sb in the cubic Ag lattice is precipitated [45]. According to the phase diagram (see. Fig. 8), this phase should be hexagonal with the space group $P6_3/mmc$. However, during crystallization, the thermodynamic equilibrium is not reached and high pressures in and around the particles might occur, which both can affect the real positions of the phase stability areas depicted in Fig. 8. Furthermore, the small crystallite size may also favor other phases which as a bulk phase would not be thermodynamically stable. During the second step of thermal treatment at 760 °C (temperature T_2 in Fig. 8), this phase is no longer stable and according to the phase diagram, should decompose to cubic Ag (space group $Fm\bar{3}m$) and a liquid enriched in Sb (see arrows in Fig. 8). This should take place above the decomposition temperature T_d, which is also marked in Fig. 8. The morphology of the metallic particle is still plate-like. The simultaneously formed liquid should occur at the surface of the metallic particle and here a shell of approximately constant thickness should be formed. This shell should be enriched in Sb, whereas the inner core contains only a comparatively small amount of Sb due to the maximum solubility of 8 at% for antimony in the silver lattice.

The composition of the shell in comparison to that of the parent glass, determined by (TEM)EDXS measurements, is reported in Ref. [5]. From this quantification (1.3 BaO·0.5 SrO·71.7 ZnO·20.7 SiO_2·0.26 Ag_2O·5.54 Sb_2O_3) as well as the results presented in Figs. 2 and 3, it can be concluded that the EDXS analysis of the core is attributed to a crystalline oxidic phase with Zn, Si, and Sb as main constituents. The occurrence of Sb in the shell is already described above. A similar principle might explain the enrichment of zinc in the shell. Metallic zinc, which may be formed in silicate glasses, (see e.g. ref. [46]) can be dissolved into the metallic silver lattice, even in high concentrations [47]. Upon cooling, the solubility of zinc in silver becomes lower and zinc is expelled from the Ag-lattice. In literature, a ternary oxidic compound containing Zn, Si, and Sb is not described. The only Zn- and Si-containing compound, stable at ambient pressure is willemite (Zn_2SiO_4). Nevertheless, the shell also contains Sb, which as described above, may occur in the oxidation states Sb^{III} and Sb^{V} which possess ionic radii of 76 and 60 pm, respectively. Zn^{2+} and Si^{4+} possess ionic radii of 60 and 26 pm, respectively. It is well-known that Zn in willemite might be substituted against other divalent transition metals, such as Mn^{II} [48], which possess similar ionic radii. In principle, Zn^{II} might partially be substituted by Sb^{III} or Sb^{V}. It is not sure, however, in which oxidation state antimony occurs in the shell.

The other possibility is that the phase of the shell is a binary compound in the system $ZnO/Sb_2O_{3/5}$, in which Si^{IV} is incorporated. Here two binary compounds are found in the literature: $Zn_7Sb_2O_{12}$ and $ZnSb_2O_4$. The latter phase contains Sb^{III} and is tetragonal with the space group $P4_2/mbc$ (135). $Zn_7Sb_2O_{12}$ solely contains Sb^{V} and is cubic with the space group $Fd\bar{3}m$ (227). In this structure, the tetrahedral sites are occupied by Zn while the octahedral positions are occupied by Zn as well as by Sb. It can be described as follows: $(Zn)_t(Sb_{0.667}, Zn_{1.33})_oO_4$. The empirical formula according to the EDXS analyses of the shell surrounding the metallic Ag core is $Si_{0.583}Zn_2Sb_{0.33}O_4$. The observed chemical composition, however, assuming Si to occupy tetrahedral sites and

the residual tetrahedral sites being occupied by Zn, and the octahedral sites being occupied by both Zn and Sb, the stoichiometry can be described as follows: $(Si_{0.583}, Zn_{0.417})_t(Sb_{0.33}, Zn_{1.583})_oO_4$. There are additional 0.0814 vacancies at octahedral sites. The Kröger-Vink notation is hence as follows:

$0.583Si_{Zn}^{\circ\circ}$, $0.253Zn_{Sb}'''$, $0.0814V_{Sb}''''''$.

In summary in the silver- and antimony containing glass, the following reactions take place:

I During heating of the glass melt (fining reaction at low viscosities). Oxygen bubbles are formed and Sb^V is transformed to Sb^{III}: $2Sb^{5+} + 2O^{2-} \rightleftarrows 2Sb^{3+} + O_2$ (1)

II At the lower heat treatment temperature (700 °C) nucleation takes place. Sb^{III} reduces Ag^+ to metallic Ag and Sb^V is formed. The gold atoms cluster during thermal treatment just above T_g and hence form nanoparticles: $2Ag^+ + Sb^{3+} \rightleftarrows 2Ag + Sb^{5+}(3) - (1) = (6)$
Sb^{III} may also undergo a disproportionation into metallic Sb and Sb^V.
$5Sb^{3+} \rightarrow 3Sb^{5+} + 2Sb$ (10)
Sb and Ag form a hexagonal alloy with a plate-like morphology.

III At the higher heat treatment temperature (760 °C). This temperature is above the stability range of the hexagonal compound which hence decomposes into a cubic solid solution of metallic Ag with small amounts of Sb and possibly some Zn. Some of the Sb and Zn is expelled and afterward oxidized by Sb^V present in the residual glass phase. Then around the metallic Ag particle, a solid oxidic shell containing Sb, Zn, and also Si is formed. Those crystals are necessary to trigger volume crystallization of LEAZit crystals.

The formation of the core–shell structure is quite essential to achieve an effective formation and hence a high crystal density of the low thermal expansion phase. This is only possible in Ag_2O doped glasses since, in contrast to Au and Pt doped samples, only in this case a third phase between the metallic nuclei and the low expansion phase is formed.

The use of silver as nucleating agent together with the redox partner antimony enables to achieve a more fine-grained microstructure also in comparison to oxidic nucleation agents, such as SnO_2 [24], ZrO_2 [49], and WO_3 [50]. The formation of cracks which results from different coefficients of thermal expansion in different crystallographic directions can widely be avoided.

Conclusions

The reaction partner Sb has a very notable effect on the crystallization behavior of $BaO/SrO/ZnO/SiO_2$ glasses. In any case, the noble metal, present in an oxidation state ≥ 1, is reduced by Sb^{III}, which is the main redox state of Sb under the acting conditions.

In the case of Pt and Sb, also a part of the present Sb^{III} undergoes a disproportionation reaction, i.e. Sb^V and metallic Sb are formed. The latter forms an alloy with platinum particles, which is favored by the strongly negative Gibbs free mixing energy. The nucleating effect of Pt is strongly enhanced by the presence of Sb.

In the case of Au and Sb, an alloy is not formed, at least not to a noticeable extent. Nevertheless, Sb strongly enhances the nucleation of metallic Au nanoparticles, which are formed during cooling by a redox reaction of Sb^{III} and Au^+.

In the most interesting and complex case of Ag and Sb, during the first step of thermal treatment (the nucleation step), a hexagonal phase with the nominal composition $Ag_{0.84}Sb_{0.16}$ is formed which also shows a plate-like morphology. During the second heat treatment step, the temperature is outside the stability range of the hexagonal phase and the latter expels some Sb. After cooling, a metallic silver core with plate-like morphology is observed. The expelled Sb is enriched in a shell surrounding the metallic core. This oxidic shell also contains Si and Zn and triggers the crystallization of the LEAZit phase.

Acknowledgements

This work was funded by the German Research Foundation under Grant Number TH 2241/1-1.

Funding

Open Access funding enabled and organized by Projekt DEAL.

Declarations

Conflict of interest The authors declare that they have no known competing financial interests or personal relationships that could have appeared to influence the work reported in this paper.

References

[1] Rindone GE (1958) Influence of platinum nucleation on crystallization of a lithium silicate glass. J Am Ceram Soc 41:41–42

[2] Gonzales-Oliver CJR, James PF (1981) Influence of platinum additions on crystal nucleation rates in glasses close to the Na_2O 2CaO $3SiO_2$ composition. Am Ceram Soc Bull 60:352–352

[3] Kim HJ, Choi SC (2000) Effect of Sb_2O_3 and raw materials on the crystallisation of silver containing glasses. Phys Chem Glasses 41:55–58

[4] Vladislavova L, Thieme C, Zscheckel T et al (2019) Crystallization of $Ba_{1-x}Sr_xZn_2Si_2O_7$ from the BaO/SrO/ZnO/SiO_2 glass system: Effect of platinum and Sb_2O_3 on nucleation. J Alloys Compd 793:705–714

[5] Thieme C, Kracker M, Thieme K et al (2019) Core-shell structures with metallic silver as nucleation agents of low expansion phases in BaO/SrO/ZnO/SiO_2 glasses. CrystEngComm 21:4373–4386

[6] Rüssel C, Freude E (1989) Voltammetric studies of the redox behaviour of various multivalent ions in soda-lime-silica glass melts. Phys Chem Glasses 30:62–68

[7] Rüssel C (1990) The electrochemical behavior of some polyvalent elements in a soda-lime-silica glass melt. J Non-Cryst Solids 119:303–309

[8] Claußen O, Rüssel C (1997) Thermodynamics of various polyvalent main group elements in a borosilicate glass melt. J Non-Cryst Solids 209:292–298

[9] Duffy JA (1996) Redox equilibria in glass. J Non-Cryst Solids 196:45–50

[10] Borisov A, Danyushevsky L (2011) The effect of silica contents on Pd, Pt and Rh solubilities in silicate melts: an experimental study. Eur J Mineral 23:355–367

[11] Akai T, Nishii J, Yamashita M, Yamanaka H (1997) Chemical behavior of platinum-group metals in oxide glasses. J Non-Cryst Solids 222:304–309

[12] Paje SE, Llopis J, Villegas MA et al (1998) Thermal effects on optical properties of silver ruby glass. Appl Phys A 67:429–433

[13] Haslbeck S, Martinek K-P, Stievano L, Wagner FE (2006) Formation of gold nanoparticles in gold ruby glass: The influence of tin. Hyperfine Interact 165:89–94

[14] Wagner FE, Haslbeck S, Stievano L et al (2000) Before striking gold in gold-ruby glass. Nature 407:691–692

[15] Clauβen O, Rüssel C (1999) A voltammetric study of the Ag^+/Ag^0-equilibrium in soda-alumina-silicate melts. J Mol Liquids 83:295–302

[16] Thieme C, Görls H, Rüssel C (2015) $Ba_{1-x}Sr_xZn_2Si_2O_7$ - A new family of materials with negative and very high thermal expansion. Sci Rep 5:18040

[17] Thieme C, Rüssel C (2016) Very high or close to zero thermal expansion by the variation of the Sr/Ba ratio in $Ba_{1-x}Sr_xZn_2Si_2O_7$ - solid solutions. Dalton Trans 45:4888–4895

[18] Kracker M, Thieme C, Häßler J, Rüssel C (2016) Sol–gel powder synthesis and preparation of ceramics with high- and low-temperature polymorphs of $Ba_xSr_{1-x}Zn_2Si_2O_7$ (x=1 and 0.5): a novel approach to obtain zero thermal expansion. J Eur Ceram Soc 36:2097–2107

[19] Höche T, Gerlach JW, Petsch T (2006) Static-charging mitigation and contamination avoidance by selective carbon coating of TEM samples. Ultramicroscopy 106:981–985

[20] Kracker M, Thieme C, Thieme K et al (2018) Redox effects and formation of gold nanoparticles for the nucleation of low thermal expansion phases from BaO/SrO/ZnO/SiO_2 glasses. RSC Adv 8:6267–6277

[21] Thieme C, Kracker M, Patzig C et al (2019) The acceleration of crystal growth of gold-doped glasses within the system BaO/SrO/ZnO/SiO_2. J Eur Ceram Soc 39:554–562

[22] Rindone GE, Rhoads JL (1956) The colors of platinum, palladium, and rhodium in simple glasses. J Am Ceram Soc 39:173–180

[23] Briese LC, Selle S, Patzig C et al (2019) Depth-profiling of nickel nanocrystal populations in a borosilicate glass – A combined TEM and XRM study. Ultramicroscopy 205:39–48
[24] Thieme C, Thieme K, Kracker M et al (2021) Silver doped glasses from the system BaO/SrO/ZnO/SiO_2: the influence of Sb, Sn, and Ta on the formation of core-shell structures. Ceram Int 47:1126–1132. https://doi.org/10.1016/j.ceramint.2020.08.229
[25] Massalski TB, Okamoto H, Subramanian PR (1990) Binary Alloy Phase Diagrams, 2nd ed. ASM International
[26] Moisescu Ce (2002) Antimony in alumosilicate melts at high temperatures. PhD thesis, Jena University
[27] Schirmer H, Müller M, Rüssel C (2003) High Temperature Spectroscopic Study of Redox Reactions in Iron and Arsenic Doped Melts. Glass Sci Technol 76:49–55
[28] Kido L, Müller M, Rüssel C (2004) Redox reactions occurring during temperature change in soda-lime-silicate melts doped with copper, tin and antimony or copper and tin. Phys Chem Glasses 45:21–26
[29] Meechoowas E, Müller M, Rüssel C (2010) Redox relaxation in a sodium borosilicate glass doped with copper and arsenic, antimony, or tin. J Non-Cryst Solids 356:2528–2533
[30] Meechoowas E, Müller M, Rüssel C (2010) Redox Relaxation in Glass Melts Doped with Copper and Arsenic. J Am Ceram Soc 93:1032–1038
[31] Kido L, Müller M, Rüssel C (2006) Redox reactions during temperature change in soda-lime–silicate melts doped with copper and iron or copper and manganese. J Non-Cryst Solids 352:4062–4068
[32] Gravanis G, Rüssel C (1989) Redox Reactions in Fe_2O_3, As_2O_5 and Mn_2O_3 doped Soda Lime Silica Glasses During Cooling - a High-Temperature ESR Investigation. Glastech Ber 62:345–350
[33] Kido L, Müller M, Rüssel C (2005) Evidence of redox relaxation during thermal treatment of soda lime silica glasses doped with chromium and manganese. Chem Mater 17:3929–3934
[34] Kido L, Müller M, Rüssel C (2012) The effect of viscosity on the kinetics of redox reactions in highly viscous silicate liquids. J Chem Phys 136:224502
[35] Rüssel C (1989) Redox reactions during cooling of glass melts - a theoretical consideration. Glastech Ber 82:199–203
[36] Rüssel C (1991) Self diffusion of polyvalent ions in a soda-lime-silica glass melt. J Non-Cryst Solids 134:169–175
[37] Clauβen O, Rüssel C (1997) Self diffusion of polyvalent ions in a borosilicate glass melt. J Non-Cryst Solids 215:68–74
[38] Rüssel C, Kohl R, Schaeffer HA (1988) Interaction between oxygen activity of Fe_2O_3 doped soda-lime-silica glass melts and physically dissolved oxygen. Glastech Ber 61:209–213
[39] Kim W-S, Chao GY (1990) Phase relations in the system Pt-Sb-Te. Can Mineral 28:675–685
[40] Chevalier P-Y (1989) A thermodynamic evaluation of the Au-Sb and Au-Tl systems. Thermochim Acta 155:211–225
[41] Lumeau J, Glebova L, Glebov LB (2008) Influence of UV-exposure on the crystallization and optical properties of photo-thermo-refractive glass. J Non-Cryst Solids 354:425–430
[42] Glebov LB (2007) Photosensitive holographic glass - new approach to creation of high power lasers. Phys Chem Glasses: Eur J Glass Sci Technol B 48:123–128
[43] Lee B-Z, Oh C-S, Lee DN (1994) A thermodynamic evaluation of the Ag-Pb-Sb system. J Alloys Compd 215:293–301
[44] Premović M, Minić D, Manasijević D et al (2013) Experimental investigation and thermodynamic calculations of the Ag–Sb–Zn phase diagram. J Alloys Compd 548:249–256
[45] Rüssel C, Thieme C, Thieme K Verfahren zur Herstellung einer Glaskeramik und Glaskeramik, DE102018221827A1
[46] Pascual MJ, Guillet A, Durán A (2007) Optimization of glass–ceramic sealant compositions in the system MgO–BaO–SiO_2 for solid oxide fuel cells (SOFC). J Power Sources 169:40–46
[47] Gómez-Acebo T (1998) Thermodynamic assessment of the Ag-Zn system. Calphad 22:203–220
[48] Ahmadi TS, Haase M, Weller H (2000) Low-temperature synthesis of pure and Mn-doped willemite phosphor (Zn_2SiO_4:Mn) in aqueous medium. Mater Res Bull 35:1869–1879
[49] Vladislavova L, Thieme C, Rüssel C (2017) The Effect of ZrO_2 on the crystallization of a glass in the System BaO/SrO/ZnO/SiO_2: Surface versus bulk crystallization. J Mater Sci 52:4052–4060. https://doi.org/10.1007/s10853-016-0667-0
[50] Thieme C, Erlebach A, Patzig C, Thieme K, Sierka M, Höche T, Rüssel C (2018) WO_3 as a nucleating agent for BaO/SrO/ZnO/SiO_2 glasses: experiments and simulations. CrystEngComm 20:4565–4574